

Two dimensional multiscale PIV measurements within a three-phase bubble column with dual aeration plug system

Bernhard König^{1,*}, Stefan Puttinger¹, Stefan Pirker¹

¹Department of Particulate Flow Modelling, Johannes Kepler University of Linz, Austria
*corresponding author: bernhard.koenig@jku.at

Abstract Measurements within bubble columns are interesting to understand the dynamic processes in such systems. As the dispersed phase is often problematic for measurement systems the flow situations (especially with high introduced gas rates) are still a challenging field. The industrial background for this work is the ladle stirring during steel production. This paper presents the experimental setup for substituting such systems in a big scaled lab experiment including an overlaying liquid phase (substituting the slag). The target of turbulence analysis and global mixing investigation requires the observation of both, the complete setup cross section (at adequate time and spatial resolution) and a local higher resolution area in time and space. In both cases the discrimination of the involved phases needs to be performed to assure minimal spurious vectors in the PIV calculations. A procedure for separating both observation areas as well as an algorithm for separating the tracer particles (visualising the liquid phase) is presented. A concluding ensemble averaged velocity vector plot is illustrated to prove the applicability of the complete method and give an impression of the flow field within the vessel.

Keywords: 3-phase bubble column, converter stirring, alternative aeration, optical separation, algorithmic phase separation, slag substitution

1 Introduction

Multi phase systems like bubble columns are highly used in industrial processes across various branches. As the flow situation within these vessels usually affects the efficiency significantly the investigation of these systems is of great interest. This work focuses on the steel industry where the converter and ladle stirring process represents the main background. In general these processes consists of a basin filled with liquid metal and an overlaying thin slag layer as continuous phases. The discontinuous phase is introduced as gas from the bottom (or from the top like in the BOF process) of the vessel via porous plugs where it forms bubbles. These rising bubbles act in a two fold way (beside the chemical effects which are not considered herein). On one hand they induce a convective flow within the liquid phase and thus enhance the mixing and homogenisation while on the other hand non metal inclusion are guided to the slag layer where they are accumulated. Unfortunately this desired aspects are also accompanied by negative effects. The induced convective flow for example introduces shear forces at the vessel walls and the interface between steel and slag. These relative movement consequently augment the erosion of the refractory material and enhance a phenomena called slag entrainment. This effect appears when the relative motion between the two liquids triggers instabilities (e.g. Kelvin-Helmholz instabilities or vortices near the surface) with subsequent rupture of the interface and was already reported in the 1970s [1],[2]. The droplets are formed with a brought size distribution and while the bigger droplets float and reunite quickly with the top slag layer the lifetime of small droplets within the liquid metal can be significant. Furthermore, once the formation of small droplets has taken place they are prone to be dragged down by the convective flow and therefore be distributed over the whole domain. These impurities will reduce the quality of the final product. To avoid or reduce these negative effects while maintaining good homogenisation of the liquid specific methods are required. A common approach is to use multiple porous plugs at an alternating or variable operation. The underlying idea is the avoidance of a high-intensity vortex which in worst case is located near the vessel walls. Such vortices, however, are facilitated by the use of one single porous plug. The usage of multiple alternating operated plugs is capable of preventing the formation of large scale flow structures and distributes the introduced kinematic energy to smaller and more equally distributed vortices. Furthermore, this method offers a new intervention opportunity by adjusting the activation times of the plugs. This parameter and its influence on the global mixing and erosive potential requires dedicated measurement methods and postprocessing steps which represents the main focus of this work.

Obviously the conditions provided by liquid metals are some sort of disadvantageous for measurements. Experiments are therefore commonly performed within a cold air-water-oil setup substituting gas-steel-slag. A great amount of experimental research has been done for two phase flows (neglecting the slag phase) or gas-liquid-solid reactors. An overall review of measurement techniques for these systems can be found in [3]. The target of enhancing the mixing behaviour while reducing the negative effects is based on the proper analysis of turbulent flows which in turn demands high spatial and temporal resolution. Consequently point-wise measurement methods like Laser Doppler Anemometer (LDA) are not perfectly suited for the claimed task. Optical methods like Particle Image Velocimetry (PIV), Laser Doppler Anemometry (LDA) or Phase Doppler Anemometry (PDA) are aggravated by the strong physical discontinuities within bubble columns. The optical diffraction and refraction of the dispersed bubbles limits these procedures to a rather small gas hold up of about 10-19% [4]. Insensible to these optical limitations are for example techniques like the computer-automated-radioactive-particle-tracking (CARPT) or computer tomography (CT) systems. Lin et al. [5] developed the CARPT technique for solids motion in fluidised beds which was also applied to liquid motion by Devanathan et al.[6]. It utilises a radioactive material encapsulated within a synthetic housing which is tracked by several γ radiation sensors over a long period of time (~ 20 h). A problem with CARPT is the lack to measure velocities at two separated positions synchronously since it represents a Lagrangian technique with only one tracer. This would be interesting for example to calculate turbulent length scales. Another problem is that it only acquires the liquid phase, offers no information about the gas phase and their interaction, and is not able to discriminate between the two liquid phases at all.

Tomographic methods often use medical equipment and are based on X-rays[7], γ -rays[8], magnetic resonance [9] or electrical capacitance[10, 11]. Usually these systems acquire a slice of the test section and are then rotated or traversed axially to yield 3d data. Those systems are not hindered by high gas holdups nor by opaque liquid conditions. Beyond the enormous costs and complexity they prove rather weak temporal and/or spatial resolution for the targeted bubble column size.

As mentioned before the mixing of the whole column is a desired measure which requires a system capable of acquiring the whole domain while maintaining adequate resolution in time and space. PIV as stand-alone but also in combination with shadowgraphy is able to fulfil these criteria and is in contrast to tomographic techniques rather inexpensive and easy to handle. The limitation of low gas hold ups is presently an inevitable compromise, but the ability to capture both phases synchronously is beneficial and rarely possible with other techniques. Moreover, it is worth mentioning that also the third phase (oil) can be captured at the same time without dramatic increase in complexity. These characteristics makes PIV the method best suited for our requested tasks. The main difference in most of literature concerning the application of PIV to bubble columns is the type of separation procedure used to discriminate the different phases. Several methods are reviewed in the paper of Sathe [12] and shall also be mentioned shortly herein.

Two main techniques for separating the gas phase and the tracer particles within the liquid phase can be named. The first can be called an algorithmic phase separation and the second optical discrimination. Algorithmic setups are mostly based on image processing algorithms and separate the phases by either:

- size (tracers are usually very small compared to bubbles)
- slip velocity (bubbles rise faster than the fluid which can be detected as a second correlation peak [13])
- colour/grey gradient differences in combination with shadowgraphy [14, 15]

Out of focus bubbles acquired with shadowgraphy are separated by utilising a narrow depth of focus lens. The bubbles out of focus then appear with blurred edges and can therefore be detected by the algorithm.

Optical discrimination systems frequently use any kind of optical separation of tracers and gas phase. Light induced fluorescence (LIF) for example accounts for the frequency shift between irradiated and reflected light of some materials. Equipping the cameras with dedicated optical filters fulfil the separation process without any post-processing efforts [4], [12], [16].

As the analysing procedure requires the monitoring of the whole basin with best possible resolution and because the introduced bubbles are significantly bigger than the tracers used, the setup chosen for separation is of the algorithmic type. The very details of the measurement apparatus and discrimination procedures will be described within the next section.

2 Methods

2.1 Experimental setup

The main part of the experimental facility is represented by a lab scale water basin with a base area of 1x0.5 m with 0.91 m quiescent water fill level and a 0.03 m oil layer atop (see Fig. 1). Since the global flow field and the turbulent quantities therein are of major interest the whole basin cross-section needs to be observed with best possible resolution. The global view acquisition is realised with two adjacent double-frame PIV cameras (LaVision ImagerIntense, Camera 1 and Camera 2 in Fig. 1) monitoring the left and right section synchronously at a frame repetition rate of 4 Hz and 30 ms between the correlation frames. To illuminate the global view, a pulsed frequency doubled Nd:YAG laser is emitting green (532 nm) light from beneath. The illuminated plane is set to a depth of $z=-0.2$ m with the coordinate system at the left bottom corner. This plane is chosen right in front of the porous plugs which are located at $z=-0.25$ m and at a horizontal position of $x_1=0.25$ m and $x_2=0.75$ m. The shift of the illumination plane towards the front window was set to reduce the data loss of the continuous phase due to the dense bubble swarm and was thought as an acceptable trade off between data loss and mid-plane observation. Both cameras have a scaling factor of 1.17 Px/mm and a resolution of $1376 \times 1040 \text{ Px}$. To achieve a better spatial and temporal resolution in a special area of interest a third camera (PointGrey Grasshopper3, Cam 3) is added. Since the pulsed Nd:YAG laser is limited in its temporal capability an additional continuous wave (cw) laser is emitting blue (445 nm^1) light to illuminate the special area of interest. The change of laser wavelength between global view and area of interest reflects the necessity of constant illumination at every frame of camera 3 and a homogeneous illumination of camera 1 and 2. The discrimination of both laser sheets is achieved by adding optical filters in front of the dedicated cameras which finally complete the optical setup. Both laser sheets were aligned carefully to illuminate the same plane but slight differences due to different beam divergences was inevitable. Camera 3 is operated at a resolution of $2048 \times 2048 \text{ Px}$ yielding a scaling factor of 2.69 Px/mm at a frame rate of 12 Hz. The need of storing the huge amount of data directly to a hard drive prohibits higher frame rates.

The basin is filled with deionised water at a temperature of 294 K and a conductivity of $253 \mu\text{S/m}$. The seeding density was set to 0.013 g/l giving barely enough tracers per interrogation window (approx. 10 Tracer/it.win.) to reduce spurious vectors [17] while minimizing the influence of bubble mobility due to tracer accumulation on the front bubble-surface.

Pressurised air is introduced via magnetic valves and a variable area flow meter at a flow rate of 16 standard litres per minute. The magnetic valves are alternately activated by a bistable multivibrator circuit to achieve a constant switching of the aeration plugs. Each porous plug spans an area of 0.04×0.04 m, is made of foam, and generates heterogeneous bubble sizes between 3 mm and 12 mm^2 with its size distribution maximum at around 5 mm. Note that this is just a rough estimation due to evaluation only within a 2d slice of few images and is mentioned solely for getting a better overview of the input parameters.

Paraffinum liquidum is used as the third phase oil layer. This oil was chosen to fit a certain similarity criteria to scale the real process. The decisive parameters for a meaningful scaling was thought to be the density, viscosity, and surface tension ratios between the two continuous phases. Therefore, physical parameters for an ordinary steel/slag combination were found in Mills^[18] and summarized with the water/oil parameters in Table 1. An exact match of every parameter ratio were not possible. To obtain a useful scaling number anyway the parameter ratios was chosen to yield a similar Laplace number:

$$\text{La} = \frac{\text{Re}^2}{\text{We}} = \frac{\sigma \rho L}{\eta^2}. \quad (1)$$

Substituting the parameter ratios into the Laplace number and using the height of slag divided by the height of liquid steel as the length scale ratio L specifies paraffinum liquidum as a suitable slag analogon. Both ratios,

¹The wave length was chosen to 445 nm since the Sony ICX625 CCD chip has its peak quantum efficiency between blue and green.

²Since the bubbles are rather big (>3 mm) they appear not spherical anymore. However, the reported diameters herein are intentionally not Sauter-Mean-Diameters etc. because only 2d size information was available. The size mentioned here is the length of the major axis of the ellipse.

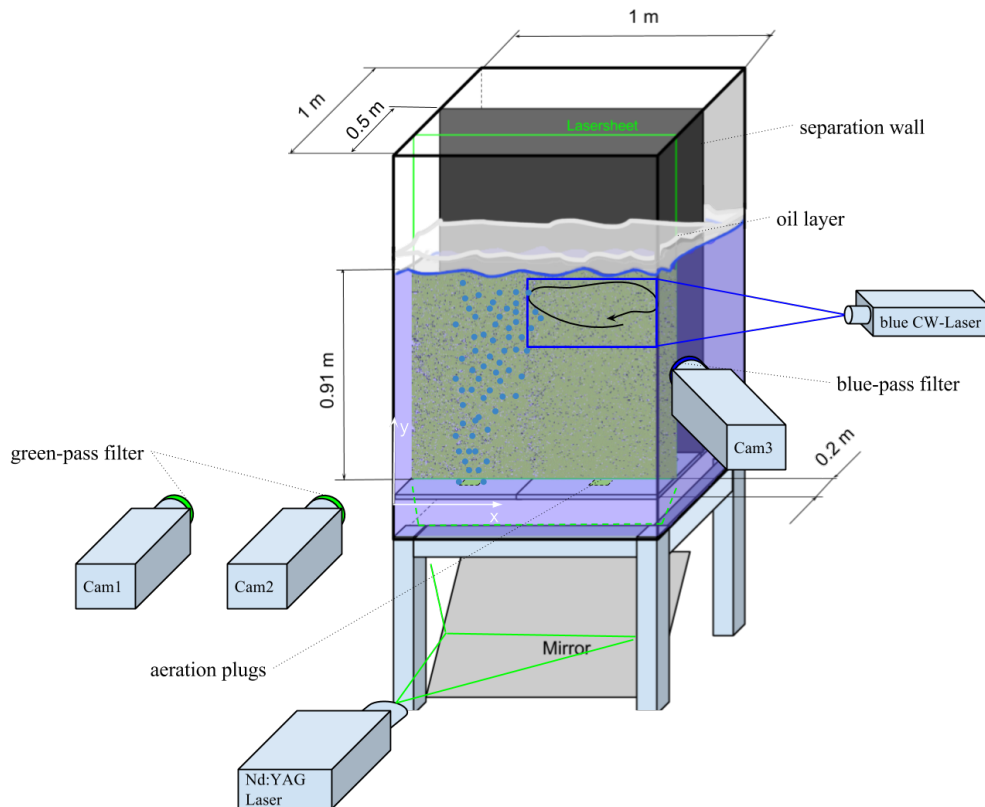


Fig. 1 Schematic of the used experimental apparatus.

slag/steel and oil/water, result in a good similarity of $La_{slag/steel} = 3.29^{-7}$ and $La_{oil/water} = 3.18^{-7}$ getting a reasonable 3% relative difference.

Paraffinum liquidum is a transparent liquid which need to be coloured in a way to be visible and discriminable from the water on all cameras (through all optical filters). A certain trade-off was made between opacity and full opaqueness to ensure good visibility while not absorbing/reflecting the whole laser light. This would result in a 'glowing' oil layer including all the negative effects for image acquisition. The oil was coloured by using 5 ml of oil-colour within a total amount of 15l paraffinum liquidum. This tiny amount of <1 per mill additive is assumed to not change the physical properties of the oil.

Table 1 Physical properties of used continuous phases

| Liquid steel | | | Slag | | | Water | | | Paraffinum Liquidum | | |
|--------------------------|------------|-------------------|--------------------------|-------|-------------------|------------------------|-----------|-------------------|------------------------|-----------|-------------------|
| $\eta_{1673^{\circ}C}$ | 6.1^{-3} | Pa s | $\eta_{1673^{\circ}C}$ | 0.448 | Pa s | $\eta_{20^{\circ}C}$ | 10^{-3} | Pa s | $\eta_{20^{\circ}C}$ | 0.189 | Pa s |
| $\rho_{1673^{\circ}C}$ | 7160 | kg/m ³ | $\rho_{1673^{\circ}C}$ | 3000 | kg/m ³ | $\rho_{20^{\circ}C}$ | 1000 | kg/m ³ | $\rho_{20^{\circ}C}$ | 863.3 | kg/m ³ |
| $\sigma_{1673^{\circ}C}$ | 1.650 | N/m | $\sigma_{1673^{\circ}C}$ | 0.5 | N/m | $\sigma_{20^{\circ}C}$ | 0.07275 | N/m | $\sigma_{20^{\circ}C}$ | 26^{-3} | N/m |

2.2 Discrimination procedure

As the spatial discrimination between the global view and the magnification camera is already performed by the optical filters solely the separation between the phases needs to be performed utilising algorithms. The bubbles appear as bright regions within the acquired images as also the tracers do. This brings the problem that the PIV correlation will compute high values for iteration-windows towards the bubble column and consequently calculate spurious vectors. To avoid this behaviour the bubbles needs to be masked to guarantee best possible results. Also liquid droplets of the oil phase should be masked implicating the only residual phase information will be caused by the tracer movement. Since the bubble movement is faster than the fluid the bubbles experience a significant displacement between two correlation frames. This displacement will obviously cause an

instationary masking which in turn will lead to spurious vectors again. A rather easy approach to handle this problem is to use the same global mask for both frames. The global mask is therefore simply the mask-union of both correlation frame masks yielding a bigger but stationary masking.

The separation between the phases utilises the fact that oil droplets and gas bubbles are significantly bigger in size than the tracer particles. Therefore, the tracers can be suppressed by applying a median filter of sufficient size. This requires that the seeding density is small enough that the median within a filter window is related to the background. The residual mask will then include only structures which are at least bigger than half the filter size and represent the dispersed phases.

An important and sometimes crucial step for every masking technique is the transformation from grayscale to binary images since an adequate threshold is required. Setting the threshold manually to a fixed value may run into problems when the light intensities change during the acquisition. As the bubble column and the opal slag layer represent dynamic reflections the global light intensities will vary. An often used method is the calculation based on the Otsu threshold [19] which represents a segmentation based on maximising the variance between background and foreground. If the acquired images are high in contrast this separation is usually great suited. However, big measurement volumes and diffuse light from the oil layer generate the problem that the available light intensity is decreased or distributed significantly and thus the contrast is reduced. This means an increasing variance of the foreground class (i.e. a brought histogram). The Otsu method is known to shift its threshold towards the class of larger variance (see [20]) resulting in a problematic separation for low contrast images. Figure 2 illustrates a comparison between the final masks (red coloured) computed by a manually set threshold and by the Otsu method. Image (a) and (c) are moreover adjusted in a way that 1% of the data is saturated at low and high intensities. As intended this modification (which represents only a stretching in the histogram) did not change the result computed with Otsu as the variances between the classes will only slightly change. Apparently the results using the Otsu method are not satisfying for the provided images as a lot of oil droplets and gas bubbles left unmasked. Anyhow, the contrast adjusting step delivers the solution for the manual threshold value because it cancels the varying background intensities and enables the resulting procedure.

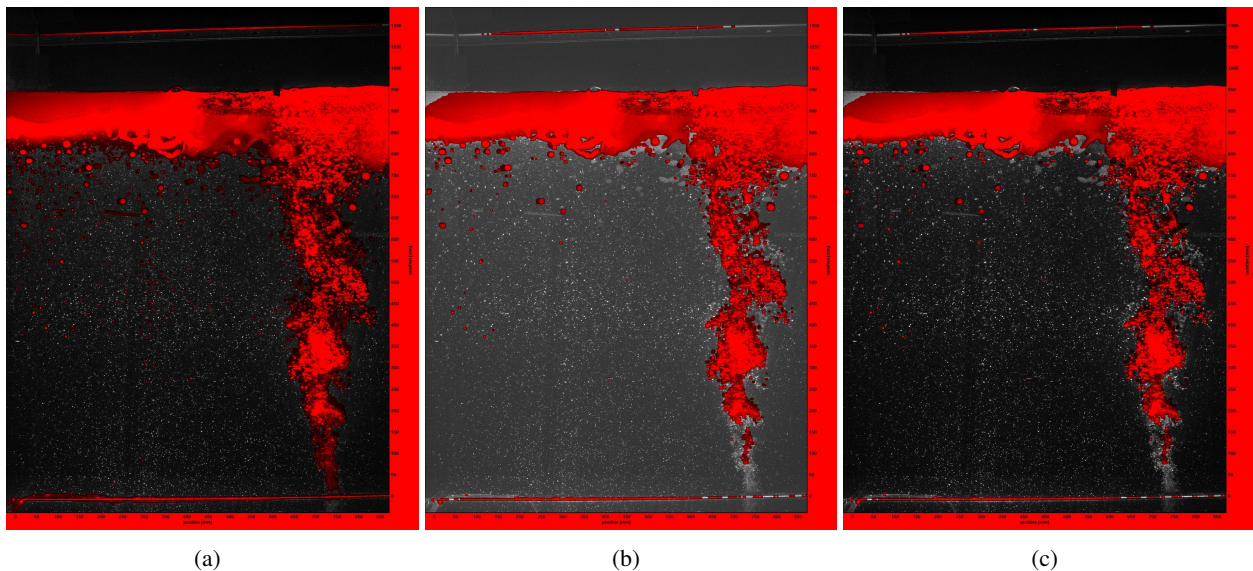


Fig. 2 Comparison of the binary image creation with threshold set (a) manually, (b) by Otsu, and (c) Otsu but with adjusted image intensities. Red colour indicates the computed binary mask which is overlaid on the source grayscale image.

3 Results

The discrimination between the different lasers was achieved without any problems by the applied optical filters and is not discussed any further. In contrast the procedure of phase separation which is applied for all

cameras should be summarised in more detail. The final procedure unite all the previous considerations and was implemented before applying the images to the PIV algorithm (see also Figure 4).

- (1) Adjusting the contrast of each image so 1% of data is saturated at low and high intensities.
- (2) Converting this image to a binary format using a threshold value of 0.2.
- (3) Suppressing tracer particles by applying a median filter with a window size of 5x5 pixel (for Cam1 and Cam2) and of size 12x12 pixel for the magnification camera (Cam3).
- (4) The so generated mask is then dilated with a structuring element of 3 pixel in size to close small gaps and ensure the mask is of sufficient size.
- (5) All the previous steps are performed also for the second correlation frame of the dedicated camera.
- (6) Both masks are added together to the global mask which is then applied to each correlation frame.
- (7) In a final step all images are saved and supplied to LaVisions DaVis software for PIV and PTV computation of the fluid and gas phase respectively.

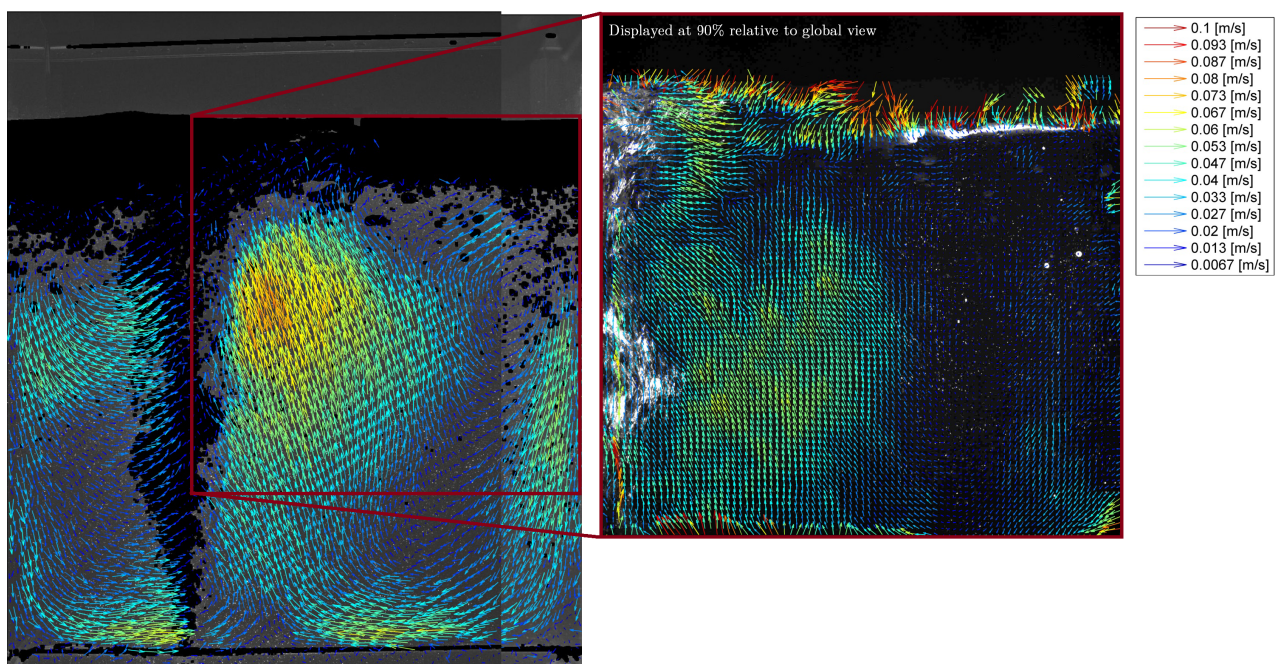


Fig. 3 Vector-plot of all cameras. The vectors represent the ensemble averaged velocities at the half activation time of the left plug. Note that the shown background image is solely displayed for estimating the aspect ratios and that the displayed *ensemble averaged vectors* can intrude the mask since the bubble column is oscillating over time.

Applying this procedure to every camera and frame, performing PIV calculations, and post-process the vector data yield the results shown in Figure 3. The subsequent processing of the vector data inherent Reynolds decomposition based on ensemble averaged mean velocities. This averaging over different realisations keeps the time dependency which is significant for such instationary processes and is the basis for all further investigations like the influence of plug switching time, erosive potential, turbulent scales, etc.

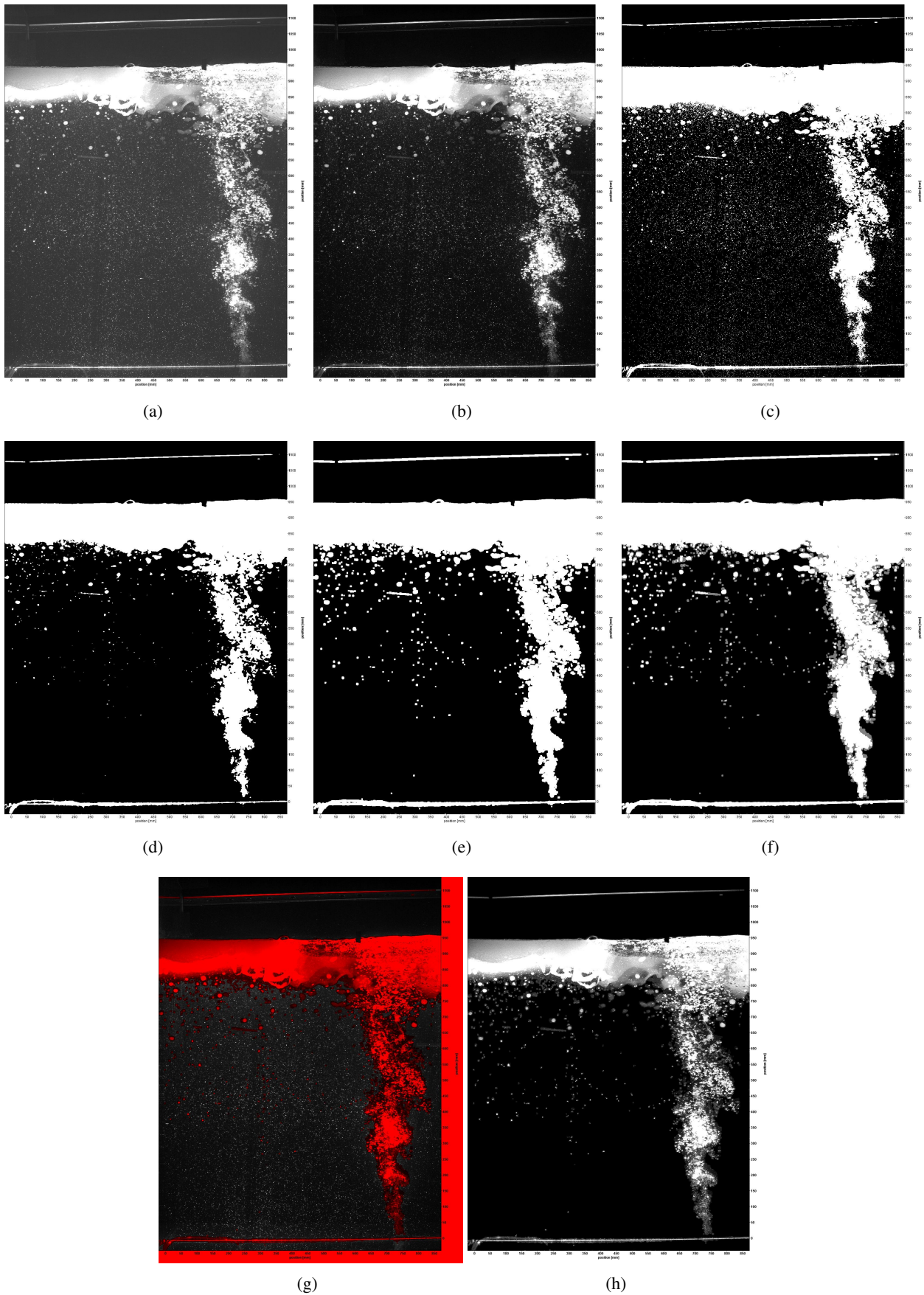


Fig. 4 Phase separation procedure. (a) Original, (b) contrast adjusted, (c) b/w computation, (d) median filtered, (e) mask dilation, (f) summation of first (gray) and second (white) frame mask, (g) applied mask (red) to original image representing the liquid phase, and (h) the inverse mask representing the gas and slag phase. Note: at printed media the tracer particles within the images might not be visible. In this case please refer to the digital version.

4 Discussion

The final discrimination images (bottom row of Figure 4) show a good agreement between the mask and the dispersed phases while maintaining a small overhead due to the fast moving bubbles. The contrast adjusting step and a fixed threshold proved to be suitable even for long measurements ($\mathcal{O}(h)$) with aeration plug shifting of approximately 15 s. It should be mentioned if the measurements include strong variations of the input gas-volume-rate an adaptation of the threshold might be required. Obviously the oil and gas phase was not separated within this work as the relevance of oil entrainment within a plane remains small but future work is focusing on the amount of entrained oil within the whole volume. However, PTV of the oil and gas phase was found to work well for dispersed drops/bubbles but is crucial within the bubble column itself. This can be addressed to the fact that bubbles appear in a very dense region where it is difficult to separate one bubble from another.

Sometimes the question arises why the bubble column was not monitored with a 3d method like digital defocusing particle image velocimetry or synthetic aperture PIV. The main problem was found within the necessity of acquiring a lot of plug switching cycles to be able to perform ensemble averaging of the velocities for turbulence analysis. The time for capturing enough realisations was about one hour of acquisition time. Already the used cameras was producing an extraordinary amount of data which would even be multiplied by 3d methods and thus go far beyond reasonable scales.

The presented method proved to be nicely applicable and resulted in a computationally fast separation procedure. The resulting mask can be easily used as algebraic mask within the PIV software (Lavisions DaVis) and for the subsequent analysis (Reynolds decomposition, turbulence analysis) of the vector data.

References

- [1] Pickering F.B. (1979) The Origin of Non-Metallic Inclusions during Steelmaking [B]. Inclusions Institution of Metallurgists, Monograph No 3: 73-93.
- [2] Asai, S., Kawachi, M., Muchi. (1983) Mass transfer rate in ladle refining processes. SCANINJECT III, Refining of Iron and Steel by Powder Injection. Carlsson: MEFOS: Lulea, Sweden, vol. 12: 1-29
- [3] Boyer C., Duquenne A., Wild G. (2002) Measuring techniques in gas-liquid and gas-liquid-solid reactors. Chemical Engineering Science, vol. 57, pp. 3185-3215.
- [4] Bröder S., Sommerfeld M. (2002) An advanced LIF-PIV system for analysing the hydrodynamics in a laboratory bubble column at higher void fractions. Experiments in Fluids, vol. 33, 826-837.
- [5] Lin J.S., Chen M.M., Chao B.T. (1985) A novel radioactive particle tracking facility for measurement of solids motion in gas fluidized beds. AIChE Journal, vol. 31, 465ff
- [6] Devanathan N., Mosleimian D., Dudukovic' M.P. (1990) Flow mapping in bubble columns using CARPT. Chemical Engineering Science, vol. 45, 2285-2291.
- [7] Seeger A., Affeld K., Goubergrits L., Kertzscher U., Wellnhofer E. (2001) X-ray-based assessment of the three-dimensional velocity of the liquid phase in a bubble column. Experiments in Fluids, vol. 31, 193-201.
- [8] Kumar S.B., Moslemian D., Dudukovic M.P. (1996) A gamma-ray tomographic scanner for imaging voidage distribution in two-phase flow systems. International Journal of Multiphase Flow, vol. 22, 108-108(1), Supplement 1.
- [9] Elkins C., Alley M. (2007) Magnetic resonance velocimetry: applications of magnetic resonance imaging in the measurement of fluid motion. Experiments in Fluids, vol. 43, 823-858.
- [10] Huang S, Plaskowski A., Xie C., Beck M. (1988) Capacitance based tomographic flow imaging system. Electron. Lett., vol. 24(7), 418-419.
- [11] Huang S, Plaskowski A., Xie C., Beck M. (1989) Tomographic imaging of two-component flow using capacitance sensors. Journal of Physics Engineering Science Instrumentation, vol. 22, 173-177.

- [12] Sathe M. Thaker I. Strand T. Joshi J. (2010) Advanced PIV/LIF and shadowgraphy system to visualize flow structure in two-phase bubbly flows. *Chemical Engineering Science*, vol. 65, 2431-2442.
- [13] Delnoij E., Kiupers J., Swaaij V., Westerweel J. (2000) Measurement of gas-liquid two-phase flow in bubble columns using ensemble correlation PIV. *Chem. Eng. Science*, vol. 55, 3385-3395
- [14] Lindken R., Merzkirch, W. (2002) A novel PIV technique for measurements in multiphase flows and its application to two-phase bubbly flows. *Experiments in Fluids*, vol. 33, 814-825.
- [15] Bröder D., Sommerfeld M. (2007) Planar shadow image velocimetry for the analysis of the hydrodynamics in bubbly flows. *Measurement Science and Technology*, vol. 18, 2513-2528.
- [16] Tokuhiro A., Maekawa M., Iizuka K., Hishida K., Maeda M. (1998) Turbulent flow past a bubble and an ellipsoid using shadow-image and PIV techniques. *International Journal of Multiphase Flow*, vol. 24, 1383-1406.
- [17] Keane R.D., Adrian R.J. (1992) Theory of cross-correlation of PIV images. *Applied Scientific Research*, vol. 49, 191-215.
- [18] Mills K. (2011) The estimation of slag properties. *Proceedings of the Southern African Pyrometallurgy*.
- [19] Otsu N. (1979) A Threshold Selection Method from Gray-Level Histograms. *IEEE Transactions on Systems, Man, and Cybernetics*. vol. 9(1),62-66.
- [20] Xu X., Xu S., Jin L., Song E. (2011) Characteristic analysis of Otsu threshold and its applications. *Pattern Recognition Letters*, vol. 32, pp 956-961. doi:10.1016/j.patrec.2011.01.021